In Situ Observation of the Motion of Platinum and Gold Single Atoms on Graphene using Aberration-Corrected Electron Microscopy

Akio Suzuta[†+], *Kenji Yamazaki*[‡], *Kazutoshi Gohara*[‡], *Tsutomu Uchida*[*‡]

[†]Division of Applied Physics, Graduate School of Engineering, Hokkaido University, Sapporo 060-8628, Japan

[‡]Division of Applied Physics, Faculty of Engineering, Hokkaido University, Sapporo 060-8628, Japan

KEYWORDS: single atom, platinum, gold, graphene, STEM, continuous image, mobility

ABSTRACT

A trace method for determining the trajectories of single metal atoms dispersed on graphene was developed using scanning transmission electron microscopy (STEM) with angstrom-order accuracy. This method was applied to platinum (Pt) and gold (Au) single atoms dispersed on free-standing single-layer graphene to observe the difference in their dynamic behaviors under electron beam irradiation. High-angle annular dark-field (HAADF) imaging showed that most of the atoms were present at the nanographene edge, especially in three or higher layers of nanographene, but few on the terrace of graphene. According to trajectory analysis, approximately 80% of the Pt single atoms stayed within one atomic distance of graphene (1.4 Å) for whole observation period (40 s). Therefore, Pt continued to be stably dispersed on the graphene as single atoms. On the other hand, more than 50% of Au single atoms traveled a distance exceeding the size of the six-membered ring of graphene (2.8 Å) even within the minimum observation interval (4 s). Clearly, Au was confirmed to have a larger mobility than Pt under the same electron beam irradiation conditions, which may be one reason for the difficulty in keeping the single atom state for Au.

Introduction

Noble metal catalysts are widely used in industry owing to their high activity and/or selectivity for many key chemical reactions.[1] Platinum (Pt) and gold (Au) are particularly valuable elements. For example, Pt is considered the most efficient for hydrogen gas production technology,[2,3] such as electrolysis of water[4] and reduction of nitrobenzene molecules.[5] Au is also used for environmental issues, such as decomposition of organic substances and reduction of nitrogen oxides, and for fuel cell anode reactions.[6-9]

To increase the reactivity of these metal catalysts, it has been suggested to make the metal finer and increase the surface/volume ratio with the ultimate size being that of a single atom. The size reduction often results in intrinsic coordination sites on metal species with enhanced activity.[10-11] The size reduction also contributes to reduced costs by significantly reducing the amount of precious noble metals required.[5]

To use these single metal atoms in catalytic reactions, some supporting materials are required. Graphene is a feasible candidate[12-14] because it has a high adsorption power for metal atoms,[15] high heat and electrical conductivity,[16] and high strength.[17] It is now relatively easy to synthesize single-layer graphene using industrially established technologies, such as the chemical vapor deposition (CVD) method. [18-21]

The single metal atoms supported on graphene can be directly observed with transmission electron microscopy (TEM). Several metal atoms have been observed via TEM at room temperature, such as the Au atom,[22-25] Cr atom,[26-29] Al atom,[26] Fe atom,[27,29,30] Cu atom,[29,31] Si atom,[29,32,33] In atom,[34] Ge atom,[35] P atom,[36] and Pt atom.[4,14,21,29,33,37] These studies showed that

each of these single metal atoms has been observed at the edges of the graphene carbon network (including with defects in the case of single-layer graphene).

In these studies, it has been important to experimentally compare whether there is a difference between Pt and Au regarding the stability of the single atom state on graphene, as these are both noble metals with only one atomic number difference; this is important for advancing the development of catalysts. Several studies have reported on the atomization of Pt on graphene.[4,14,21,37] The Pt single atom is bonded to carbon atoms of the graphene edge via a 5d orbital, and the single atomic state was maintained at room temperature for more than 1 year.[14,21] The Pt–C bond strength also became more stable on N doped graphene.[4,37] However, the single atoms have been shown to agglomerate and make clusters on graphene when the number of Pt single atoms increased[14,21] and when a catalytic reaction was attempted.[38,39] Therefore, several attempts to maintain the single atomic state have been developed, such as using single atom carriers[5,40] and graphene sheet modification.[41]

Alternatively, atomization of Au is considered more difficult than Pt; thus, its observation and use have been mainly studied as a nanoparticle.[1,6,9,42] Additionally, several technologies have been developed to maintain the single atomic state by supporting Au on graphene oxide,[8,43] by storing in FeOx,[1] or by using organic solvents.[44] It has been suggested that the difficulty of Au atomization is due to the smaller interaction between the support material and the Au cluster than that with Pt; additionally, Au aggregates easily.[9,43,45]

Usually, high-magnification TEM is required to study the dynamic behavior of such single metal atoms. However, the number of atoms that can be observed simultaneously are limited.

Therefore, it is difficult to evaluate whether the observed results show the representative behavior of the single atom.

To investigate the stable existence of dispersed single metal atoms on single-layer graphene, the dynamic behavior of many single metal atoms under electron beam irradiation was observed by continuous observation using scanning transmission electron microscopy (STEM). We developed a new method for the simultaneous measurement of the movement of a single atom by in situ observation on the angstrom scale. For the single metal atoms, we used Pt and Au, which are precious metals with high utility value and only one atomic number difference. We dispersed Pt and Au single atoms by sputtering on single-layer free-standing graphene synthesized via CVD, which was established technology in a previous study.[14,20,21] Then, we analyzed how dozens of Pt and Au single atoms moved on graphene during continuous observation for 40 s and compared their stabilities in the single atomic state on graphene.

Methods

Single-layer graphene synthesis and dispersion of Pt and Au single atoms on graphene

Single-layer graphene was synthesized on copper (Cu) foil (purity: 99.8%; thickness: 25 μm; Alfa Aesar #46365) by the previously described CVD method.[14,46] Here, we briefly describe the procedure. After etching the Cu substrate with a 100 mM ammonium peroxodisulfate solution for 4 h and rinsing thoroughly with distilled water, the free-standing graphene was transferred directly onto a Quantifoil® holey carbon-supported Cu TEM grid. The graphene was verified as being single-layer by electron diffraction using TEM.

Then, Pt or Au single atoms were dispersed on graphene by plasma sputtering. A small amount of nitrogen gas in a vacuum chamber was ionized by accelerated electrons, which were extracted from a target material under sufficient applied voltage (200 V). Then, the positively ionized atoms of the nitrogen molecules in plasma sputtered the target material for 1 s. Under these conditions, we could obtain Pt atoms on graphene with an isolation of 99%.[21] The atom was identified as being Pt by electron energy loss spectroscopy (EELS). If the sputtering time was increased to increase the amount of dispersion, the Pt atoms aggregated. [14]

Because we did not have experience with Au single atom sputtering, we applied the same procedure to obtain the free-standing graphene sample using Au single atoms. The identification of Au was also achieved via EELS.

STEM observation and drift correction procedures

Single atom observation was performed using aberration-corrected STEM (JEM-ARM200F, JEOL, Ltd.) for high-angle annular dark-field (HAADF) STEM observations at 80 kV and a fixed magnification of 1.5×10^7 (15M), which allowed simultaneous observation of both single metal atoms and nanographene on graphene.[14,20,21,37] The residual vacuum level of the sample column was 1.5×10^{-5} Pa. These conditions can also reduce the damage of graphene by knock-on.[47,48]

HAADF images of the single metal atoms on graphene were obtained every 4s, which is the time resolution of this method, to determine the movement of atoms under scanning electron beam irradiation. For the case of Pt-deposited graphene sample, this time interval extended to 10 s due to the small mobility of Pt atoms. Figure 1 shows a series of HAADF images of Pt-deposited graphene. High-contrasted small (approximately 2 Å) particles (isolated Pt atoms) were dispersed across the entire area, and small islands of multilayer nanographene flakes (smoky or foggy contrasts) were stacked on single-layer graphene with low contrast as the base.

Nanographene was partially laminated on the first layer of graphene, and Pt single atoms with high brightness and a magnitude of several Å are present. Images in which single atoms were observed in the same field of view were continuously acquired. These dozens of Pt atoms were irradiated almost equally with the same amount of electron beam; thus, we analyzed the mobility of these particles simultaneously for 40 s using the following image processing procedure. Since the electron beam irradiation also affect the stability of nanographene, the longer irradiation time made difficult to distinguish the mobility of metal atoms themselves and the displacement of their binding base.

Each of the obtained images was captured as an image with 512 × 512 pixels and analyzed with an accuracy of 1 pixel (0.27 Å × 0.27 Å) at a magnification of ×15M.

During continuous observation, the observed area gradually shifted (called "drift"). Because the size of each single atom was approximately 2 Å,[21] drift correction was required for tracking the movement of this particle at the angstrom scale. In this study, angstrom-order drift correction was achieved by using the following image correlation method.

Compared to the original size (512 × 512 pixels), a smaller area (412 × 412 pixels) was selected as the reference of the first frame. This reference area was obtained by removing the surrounding edges of 50 pixels, which was approximately 10% of the area, because this edge of the image had a high probability of disappearance due to the drift in the subsequent frames. We then calculated the correlated value (R_{fg}) by the zero-mean normalized cross-correlation (ZNCC) equation (eq. (1)) between this reference area and the image data in the region from the starting point (0, 0) to the ending point (411, 411) in the second STEM frame. The detailed calculation procedures are shown in the previous work. [49]

$$R_{fg} = \sum_{x,y\in 411\times 411} \frac{(f(x,y)-\bar{f})*(g(x,y)-\bar{g}-2*MIN(g))}{\sqrt{\sum_{x,y\in 411\times 411}(|g(x,y)-\bar{g}-2*MIN(g)|^2)}*\sqrt{\sum_{x,y\in 411\times 411}\left(|f(x,y)-\bar{f}|^2\right)}} \quad (1)$$

Here, f (x, y) and $\bar{f}$ are the intensity at (x, y) and the average intensity of the first frame, respectively, whereas g(x, y), $\bar{g}$, and MIN(g) are the intensity at (x, y), the average intensity, and the minimum intensity of the target area in the second frame, respectively. Each R_{fg} value was calculated by shifting by 1 pixel in the x- or y-direction in the second frame, and we obtained

100 × 100 correlation values. The deviation from the starting point coordinates of the first frame to the starting point coordinates of the highest correlation image was defined as the drift when the second frame was acquired. This drift correction process was performed on the following 2nd and 3rd frames and the 3rd and 4th frames to obtain the drift-corrected images. Figure 2 and Supporting Information A shows an example of using the drift correction method. The validity and accuracy of this draft correction method was discussed in our previous study.[49]

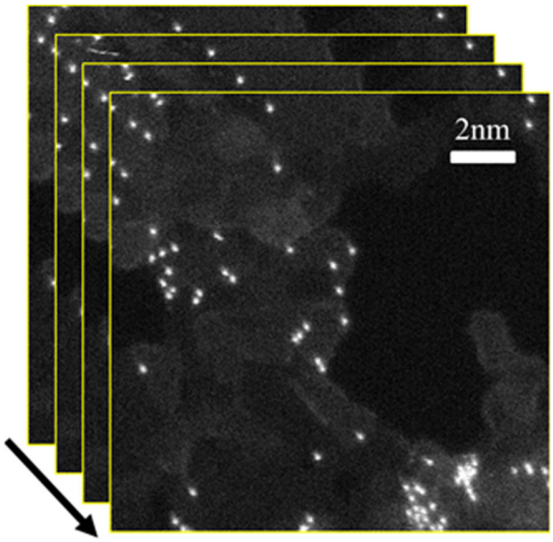

Figure 1. Example series of HAADF images for Pt-deposited graphene

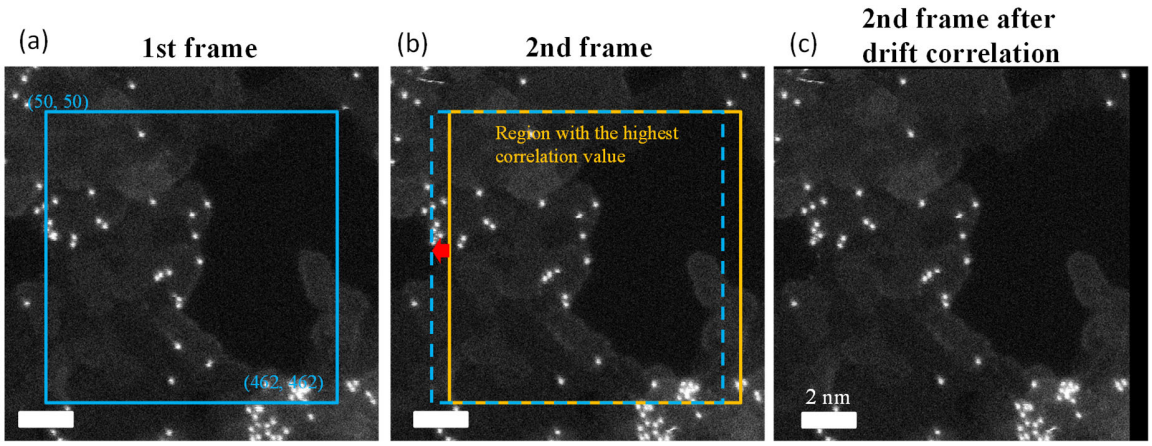

Figure 2. Example of drift correction. a) The reference area (starting point (0, 0) to ending point (411, 411)) in the first frame is shown in the blue frame. b) In the 2nd frame, the correlation with the reference area of the 1st frame was calculated, and the area with the highest correlation is shown in the yellow frame. The drift amount is shown by the difference from the reference area. c) Image with drift correction applied to the image in the 2nd frame. There was a no-image area on the right side due to the drift.

Position and size determination of a single atom

As shown in Figure 1, many bright spots are dispersed on the graphene. If a bright spot is a single Pt atom, it was shown that the intensity distribution should be able to be fitted by the Gaussian with the atomic size.[21] Using this analogy, the Gaussian was fitted for all bright spots in each image, and we determined whether the bright spot was a single atom or an aggregate of multiple atoms. We also applied this analysis to the case of Au single atom. When it was a single atom, its position coordinates were determined.

First, a STEM image (32-bit) was linearly converted to a 16-bit image for the following analyses. On the 16-bit image with a maximum brightness of 6.55×10^4, a bright spot with a brightness of more than 5×10^4 was determined to be a metal particle, and a Gaussian was fitted by our image processing program to identify a single atom from its full width at half maximum (FWHM) value. Using these criteria, the FWHM of the Pt single atom was 1.8 ± 0.1 Å, and for Au, it was 1.9 ± 0.2 Å. We confirmed that the Gaussian fitting of this Pt single atom is comparable to that of the previous study[21] and consistent with the relative Pt/Au van der Waals diameters. Additionally, when the FWHM was estimated to be apparently larger than the single atomic size or when multiple atoms were aggregated, we performed multiple Gaussian fittings. Based on this multiple fitting, the spatial resolution that could distinguish between two single atoms was estimated to be 4 pixels = 1.1 Å under the observational conditions of this study.

The position coordinates of each single metal atom identified by above methods was traced for 40 s using the Fiji plugin automatic tracking software.[50] Figure 3 shows an example of the trajectories of Pt single atoms for the images shown in Figures 1 and 2.

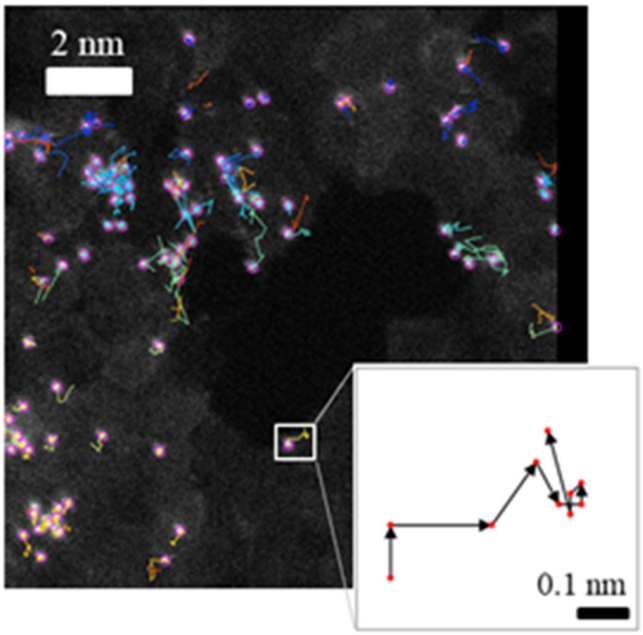

Figure 3. The position of each Pt single atom (enclosed in a square) was measured every 10 s from the drift-corrected continuous images, and the trajectory is displayed as a line. One typical trajectory is enlarged and shown on the lower right.

Evaluation of the number of layers of nanographene

Nanographene can be identified by STEM observations at an acceleration voltage of 80 kV.[14,20,21,37] As shown in Figure 1, nanographene was present on the free-standing single-layer graphene, and single Pt atoms were present on nanographene. Thus, to investigate the position of the single metal atoms on graphene, the shape and number of nanographene layers were measured.

It is well known that the HAADF intensity scales with atomic mass and material thickness.[51,52] Based on these results, image contrast was used in the previous our studies[20,21] to discriminate layer numbers of nanographene. Thus, in this study, several line profiles were measured in the first frame image, and the intensity of each nanographene layer was determined.

Figure 4 shows an example of this procedure. A line profile measured along the red line in Figure 4 (a) is shown in (b). Because the region with the lowest intensity (approximately 17 in Figure 4(b)) corresponds to the first single-layer graphene, the intensities corresponding to the 2nd and 3rd nanographene layers were obtained discretely. Two or more layers of nanographene were formed on the wide first layer in this observed area. To avoid the large background from contaminations, arbitrary three line-profiles were selected in the same image, and the intensity distribution for nanographene layers was obtained (Figure 4 (c)). This intensity distribution consisted of three Gaussian distributions with peaks at intensities of 1st, 2nd and 3rd layers in Figure 4(b), proportional to the number of Gaussian distributions. The standard deviation of each fitted Gaussian distribution was known to increase with the number of nanographene layers affected by the lamination of the carbon atoms.[20] The threshold between neighboring layers was determined as the center of these peak intensities. Since it was difficult to clearly distinguish

between nanographenes of more than 4th layers. we categorized higher layers to be “more than 4 layers”. Then, the images were categorized into 1st single-layer graphene and 2, 3, and more than 4 layers of nanographene, which are shown in the pseudo-colored map (Figure 4 (d)). By determining the shape and number of nanographene layers, and by creating continuous images, we observed changes in the shape of the nanographene layers during continuous STEM observations for 40 s and their positional relationship with single metal atoms.

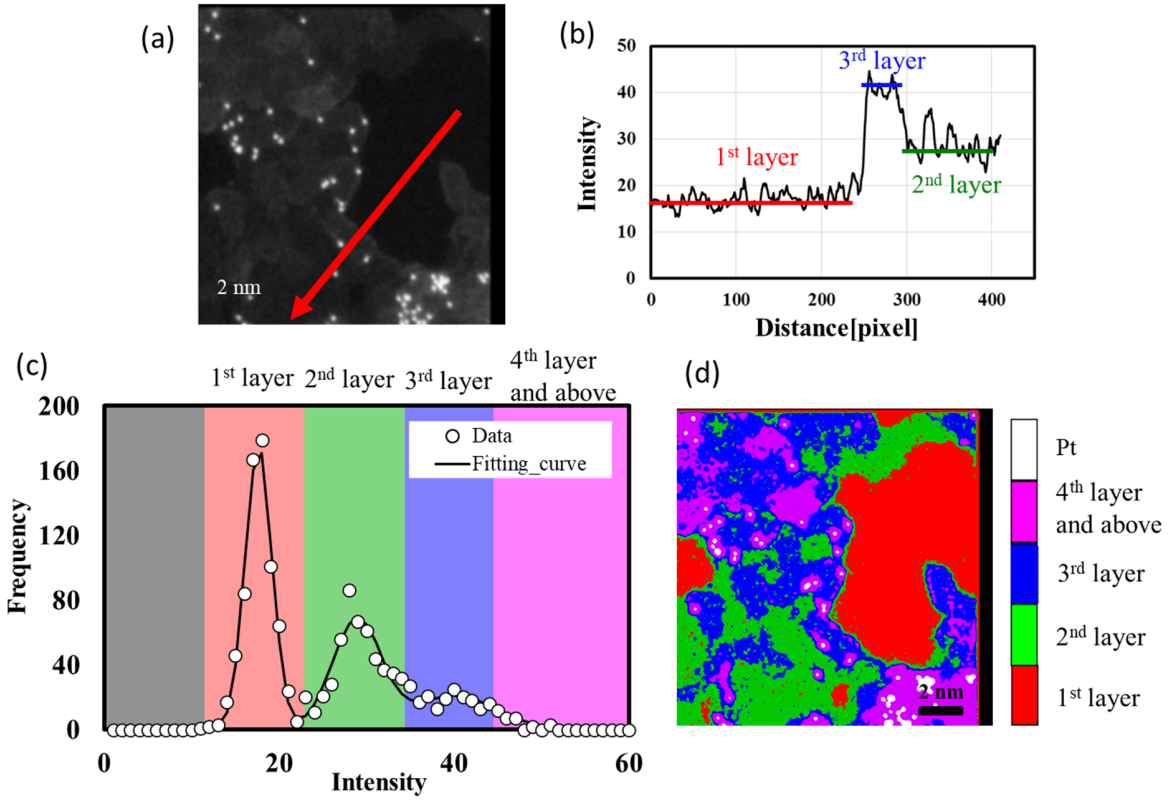

Figure 4. Example of how to obtain the shape and the number of nanographene layers. (a) Acquiring one line profile in one image and (b) its intensity profile. (c) Cumulative histogram of the three line-profiles obtained in (a). The number of nanographene layers was determined from the results of fitting up to 3 layers with a Gaussian. (d) Pseudo-colored image with the number of nanographene layers.

Results & Discussion

Continuous STEM observations

We prepared Pt- or Au-dispersed graphene transferred on the TEM grid to obtain the series of HAADF images. As shown in Figures 1 to 4, single-layer graphene and various shaped nanographene were observed in different contrasts. Additionally, many fine particles with high brightness were dispersed on the graphene. We then fitted 2-D Gaussian distribution to all observed bright spots with the fitting parameters of peak position and FWHM (see Supporting Information B). This fitting shows the minimum FWHM to be constant at approximately 2 A. This is similar to the diameters of Pt or Au single atoms, which consistent with the case of Pt single atom.[21] Although the intensity profile of single atom is a convolution between the atomic scattering potential and the probe intensity profile, the case of Pt and Au atoms are feasible for the coincidence of atomic size. Therefore, we decided the bright spot fitted with this Gaussian distribution to be the single atom. It is also found that this procedure is useful for Au single atom. This fitting procedure was also used for distinguishing atoms in the aggregated spot. The atomic species was verified by the EELS measurements, although the signal from the single atom was very small (see Supporting Information B).

Figure 5 shows the trajectories of (a) Pt and (b) Au single atoms (marked in red) on graphene for 40 s. The trajectories of all particles shown on the image are shown by the blue line, and two typical particles are selected in each image to enlarge the trajectories. In the enlarge trajectory, each arrow shows the positions of a metal atom in neighboring frame micrographs. The atom may undergo several steps during the frame time, we can observe only its final location. Therefore, we define the length of an arrow as the moving distance of this atom per

frame. Because the enlargement ratio is arbitrary, the display area is shown as a square on the image with a scale bar of 1 Å. A movie of the continuous image is provided in Supplemental Information B-1.

From these figures, we confirmed that most of the Pt and Au particles maintained the single atomic state for 40 s on graphene. In particular, the Pt particles did not move significantly in 40 s, and Au particles moved a longer distance than Pt. Additionally, as shown in the SI1 movie, the shape of nanographene changed slightly during the experiment. However, the shape change was too small to affect the metal particle movement. Thus, the movements of the single atomic particles observed in Figure 5 did not reflect the movement of the underlying nanographene; instead, they reflected the mobility of each single atom by electron beam irradiation at room temperature. Thus, the mobility of Pt single atoms differs from that of Au.

In this study, the number of nanographene layers was analyzed using the intensity information provided in the STEM image, and continuous images that identified the shape and number of nanographene layers were obtained. Figure 6 shows (a) Pt and (b) Au dispersed on graphene with pseudo-colors used to distinguish single-layer graphene (red) from nanographene (2^{nd} layer: green, 3^{rd} layer: blue, more than 4 layers: pink) and single metal atoms (white). See the movie in Supplemental Information B-2. The observed area includes both single graphene terrace (red) and island-like nanographene stacked on it. Higher-order nanographene tended to be smaller and to have a complicated shape.

Figure 6 shows that neither Pt nor Au single atoms were present on the terrace of single-layer graphene, and most of them were located at the edge of the nanographene, which has a multi-layered structure. Previous studies[21,37] reported that Pt single atoms bond to the carbon

atoms of the nanographene edge. This study not only confirmed that this was consistent with previous studies but also indicated that Au single atoms tend to be present at the nanographene edges as binding sites also. Thus, we confirmed that the nanographene edge is the main binding site for single metal atoms.

Previous studies have suggested that single metal atoms are less likely to be present on graphene terraces[33,54] and that graphene edges and defects provide stable binding sites.[25,29,31] Additionally, because single metal atoms bonded to the graphene edge show a difference in the bonding energy between the metal and carbon depending on the location,[23] a single metal atom with a weaker bond is easily broken under electron beam irradiation at room temperature; thus, it moves to the next stable binding site.[31]

In this study, there was no single metal atoms on monolayer graphene. It is likely difficult for single atoms to be present on the terrace because there were no edges in this layer. A previous study[23] suggested that a Au single atom that is present at the graphene edge has a higher binding energy than that on the graphene terrace. Thus, it is possible that single metal atoms that initially dispersed on the terrace of the monolayer graphene could not stay there under electron beam irradiation and thus moved to a more stable nanographene edge.

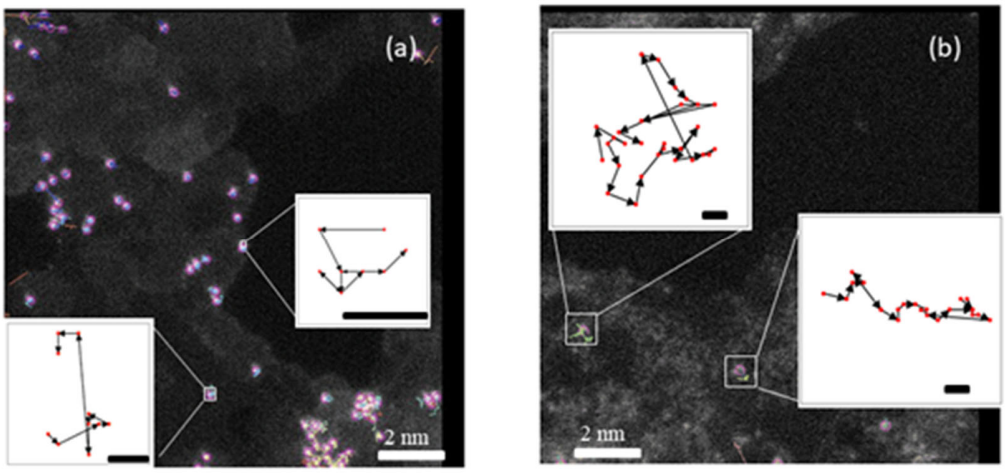

Figure 5. Typical image showing the trajectories of (a) Pt and (b) Au single atoms on graphene from a series of drift-corrected microphotographs. Two particles were selected for each image to show the enlarged trajectories (Because the enlargement ratio was arbitrary, the display range is indicated by a square, and a 1-Å scale bar is shown in each diagram.). See Supplemental Information B-1 for the movie.

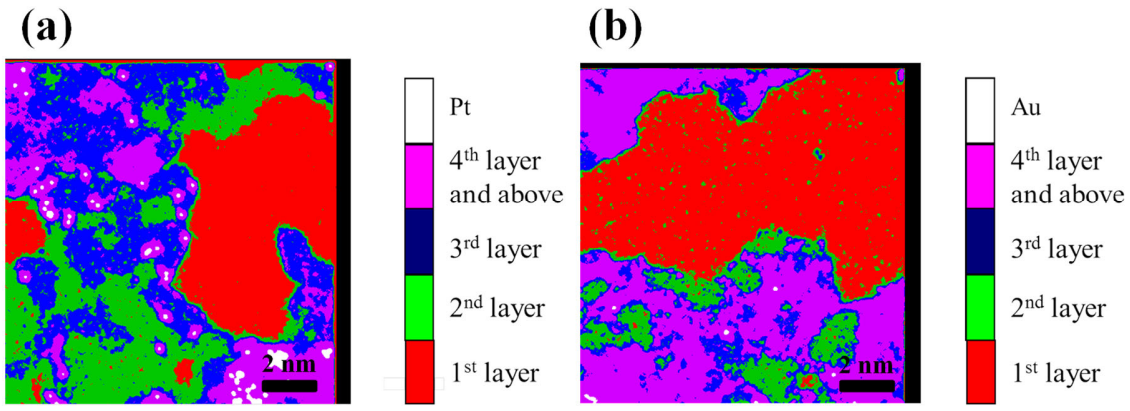

Figure 6. Pseudo-colorized images of (a) Pt and (b) Au dispersed on graphene. Because the structure of the upper layers was complicated and the number of layers could not be distinguished, we classified the (1^{st}) single graphene sheet and the number of nanographene layers into 2^{nd}, 3^{rd} and more than 4 layers of nanographene.

Dynamic behavior of single metal atoms on graphene

To quantitatively compare the movements of both Pt and Au single atoms, the average moving distances of all single atoms between the frames were calculated. Figure 7 shows the temporal change in the average moving distances of Pt (solid circles, every 10 s) and Au (open squares, every 4 s). Each error bar indicates the standard error of the average.

This figure indicates that Pt moved less than 1 Å on average in 10 s, and this did not change for 40 s. Thus, all Pt single atoms in the observed area showed similar small mobilities. The total mean value was 8.3 (± 5.4) × 10^{-12} m/s, which was smaller than the nearest atomic distance of carbon atoms constituting graphene (1.4 Å). In our previous researches[21,37], the first principle calculation was performed to investigate the local electronic state and stability of the Pt single atom bonded to the nanographene edge.

The Au single atom, however, showed a mobility that was significantly (statistically compared by the Steel–Dwass method[53]) larger than that of Pt, and that fluctuated depending on time on the particle. Because most the Au atoms were also at the nanographene edge, we considered the nanographene edge as a binding site for them as with Pt. However, the average moving distance for 4 s exceeded the size of the six-membered carbon ring (2.8 Å) of graphene, and the total mean value of all particles for 40 s was 1.2 (± 0.9) × 10^{-10} m/s. Thus, Au single atoms have large mobilities along the bonding sites of the nanographene edge under electron beam irradiation. In this study, it was clarified that the Pt atom bonded to this edge is very static. Therefore, in the future, we plan to investigate whether this bond can be broken by the energy transfer of electron beam irradiation.

To observe the movement in more detail, the moving distance between each frame by each single atom of Pt and Au was measured, and the frequency distribution that accumulated over the observation time (40 s) is shown (Figure 8). The bin of the frequency distribution was used as the spatial resolution (1.1 Å) in this study. Additionally, the number of nanographene layers in which each single atom was bound was determined. This allowed us to analyze the mobility difference for each binding location.

As shown in Figure 8 (a), approximately 70% of the Pt single atoms moved less than 1.1 Å (i.e., less than the spatial resolution) during 10 s. Considering that the nearest atom-to-atom distance of carbons in graphene is 1.4 Å, this means that Pt single atom binding at the nanographene edge does not move from the bonding site even upon electron beam irradiation. This is consistent with the observation results shown in Figure 5 (a), and a previous study[21] that reported that Pt single atoms that were dispersed on graphene maintained their single atomic state on graphene for almost one year without alteration. Therefore, this confirmed that nanographene that forms on monolayer graphene supplies a large number of binding sites for Pt single atoms and that the Pt single atoms that bind there have a high stability.

On the other hand, such stable Au single atoms are only 20% of the total particles (Figure 8(b)), and 80% of Au single atoms moved beyond 1.4A, more than 30% of all the Au single atoms moved more than the six-membered ring size of carbon constituting graphene (2.8 Å) during 4 s. Thus, Au single atoms likely bind to carbon atoms at a stable site (i.e., at the nanographene edge), but their stabilities are lower than those of Pt single atoms. A theoretical calculation of the binding energies between the metal atom and carbon atoms (C) of the graphene terrace[54] suggested that the binding energy of Pt–C was larger than that of Au–C. Thus, similar

theoretical calculation between metal atoms and the nanographene edge will reveal the difference of mobilities of metal atoms.

As shown in Figure 8, most of the Pt and Au single atoms were present at the edges of more than three layers of nanographene. Additionally, the single atoms with a large moving distance were located at the edges of nanographene with more than four layers rather than with lower layers. Thus, the single metal atoms dispersed on graphene were more bonded to the edges of the higher layers of nanographene than the lower layers, and the single metal atoms bonded to the edges of the higher layers were relatively unstable upon electron beam irradiation.

The previous EELS measurements showed that nanographene with more layers had a higher defect density than nanographene with less layers.[20] Thus, the number of sites to which single metal atoms can bind is expected to be larger in the higher layers of nanographene, and the binding force of the nanographene edge with the single metal atoms is relatively low. This may support our findings that the metal–carbon bond was broken relatively easily by electron beam irradiation and that metal atoms easily began to move or the moved metal atoms easily bonded in that location.

Assuming that single metal atoms on graphene are randomly surface-diffused from stable sites by electron beam irradiation, the mean square displacement (MSD: σ^2) of each metal atom is expected to be proportional to time. When the position coordinates (x_i, y_i) of each atom are used, σ^2 is obtained from Eq. (2).

$$\sigma^2 = \frac{1}{n}\sum_{j=1}^{n}\left(x_j^2 + y_j^2\right) \quad (2)$$

Figure 9 shows that both σ^2 of Pt and Au increase linearly with time. The rate of increase from the origin is estimated by the least square method, and it was found that of Au (1.2×10^{-2} nm^2/s) to be about an order of magnitude larger than Pt (1.0×10^{-3} nm^2/s). Since this is known to be proportional to the diffusion coefficient, it can be said that Au single atoms bound to the nanographene edge tend to move at an order of magnitude faster than Pt.

The dynamic behavior of Au single atom trapped in the single-layer graphene edge has been reported,[23] and the trajectory of a single atom under electron beam irradiation was obtained. It is difficult to make a direct comparison with this study because various conditions such as the graphene status and the electron irradiation are different, but MSD was shown to be proportional to time within the range where graphene was not damaged by electron beam irradiation (about 5 minutes). They estimated the extracted nominal diffusivity to be about 1.7×10^{-4} A^2/s. This value is four orders of magnitude smaller than the MSD of Au trapped in the nanographene edge obtained in this study. This may suggest a possibility that the Au single atom that binds to C in the single-layer graphene edge is more stable than that binds to the nanographene edge. Further experimental and theoretical studies are required to reveal this possibility.

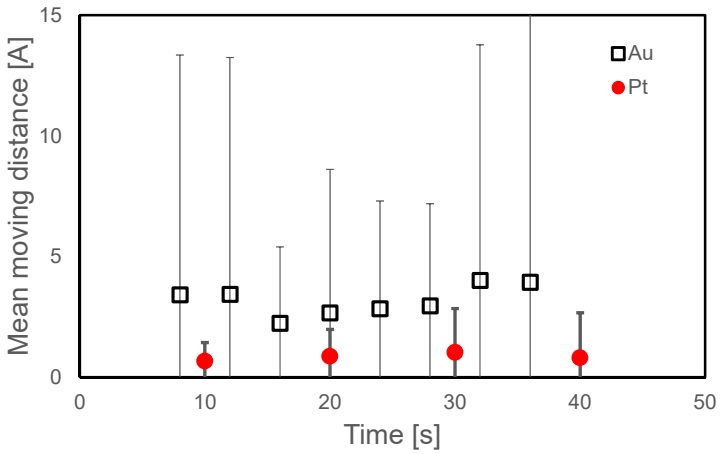

Figure 7. Average moving distance of all single atoms between each frame. Pt atoms (solid circles) were averaged every 10 s, and Au atoms (open squares) were averaged every 4 s.

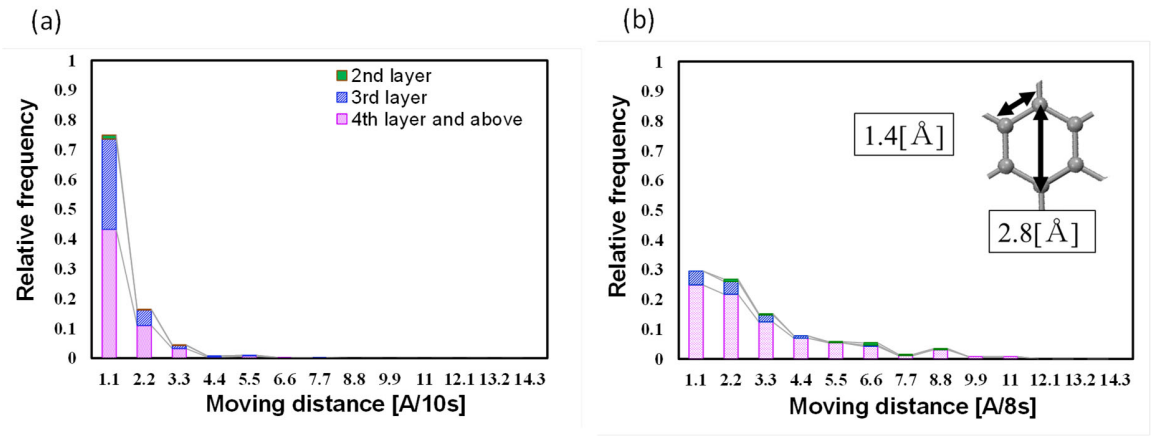

Figure 8. Cumulative frequency distribution of (a) Pt single atom moving distance during 10 s and (b) Au single atom moving distance during 4 s. Each atom was classified according to its binding site and the number of layers of nanographene. The upper right picture shows the size of the graphene six-membered ring.

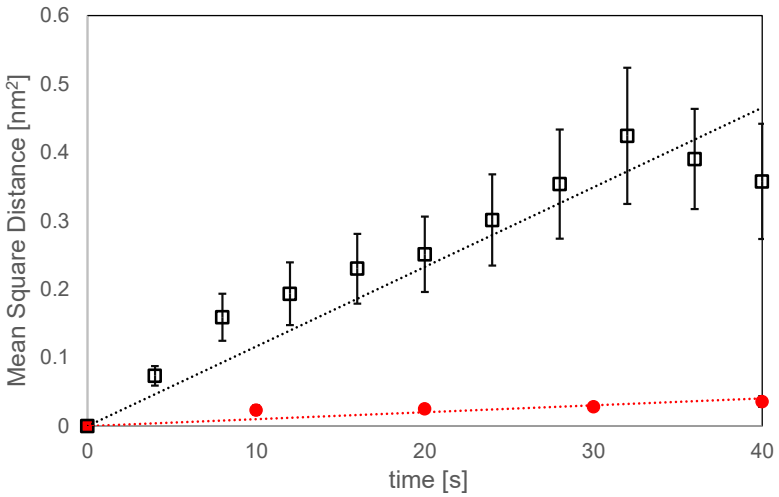

Figure 9. The mean square displacement of Pt (circles) and Au (square) single atoms on graphene as a function of time. Each error bar shows the standard error of σ^2 estimated in each frame. Dotted line shows the linear line fitted by the least square method (R^2 is 0.93 and 0.97 for Pt and Au, respectively).

Instability and aggregation of Au single atoms on graphene

As described above, our results indicate that a Au single atom is less stable on graphene than a Pt single atom. Therefore, Au atoms can move relatively easily under electron beam irradiation; thus, there is a high probability that the single atoms meet each other, and they are likely to aggregate and become nanoparticles. This is also suggested by the slightly lower magnification (×10M) of the STEM observations of Pt or Au dispersed on the graphene samples, which were sputtered under the same conditions. Figure 10 shows examples observation of (a) Pt-dispersed and (b) Au dispersed graphene, which allowed us to determine the distribution state of each metal atom over a wider area. Both metal particles were observed from the single atomic state to the aggregated state. However, compared to the Pt-dispersed sample (a), the Au dispersed sample (b) showed a larger aggregated state in which dozens of Au atoms aggregated and were of a size of approximately 1–2 nm, whereas the number of particles in the single atomic state was smaller. Because we did not have enough experience with the sputtering conditions for Au single atom dispersion on graphene, we used the same sputtering conditions as used for Pt for Au sputtering in this study. However, even for Pt sputtering, it has been found that Pt tended to aggregate more as the sputtering time increased.[14,21] Thus, although the optimal condition for Au sputtering is a remaining issue for future work, it is reasonable to conclude that Au is more likely to aggregate and form nanoparticles on graphene than Pt, at least when they are sputtered under the same conditions. We believe that the difference in single atomic mobility found in this study is one cause for the easy aggregation nature of Au single atoms.

In the case of Pt (Figure 10(a)), the majority was in a dispersed single atomic state, but some aggregates of approximately 10 atoms were also observed. Under the sputtering conditions for Pt used in this study, 99% of Pt in the observation area was predicted to be dispersed as the single

atomic state.[14,21] However, when we observed the same sample at lower magnification, we found a cohesive state depending on the location. This discrepancy with previous research can be disregarded because many of these aggregates were found to be separated into single atoms when observed at higher magnification. Whether these aggregates grow and become nanocrystallized or redispersed cannot be clarified from the scope of this study, and this remains an issue for future work.

Generally, the finer the particles, the greater the disadvantage of the surface free energy, resulting in thermodynamic instability, which leads to the aggregation and sintering of fine particles, as well as coarsening.[1] In this study, the Pt single atoms dispersed by the sputtering method on the graphene produced by the CVD method were stabilized by bonding with the carbons of graphene (or an impurity atom, such as N doped into graphene), and the single atom condition could be maintained for more than 1 year at room temperature.[21,37] Au can also be atomicized and dispersed on graphene via the same method, and Au single atoms stabilized at the edges of nanographene, which is consistent with previous work on Au single atoms located at the edges of single-layer graphene.[23] Additionally, we found that the single atoms that bonded at the nanographene edge had larger mobility than Pt. This is consistent qualitatively with the calculation that the binding energy between Au and the carbons in the graphene terraces is lower than that between Pt and carbon.[45,55] Thus, the electron beam irradiation energy is sufficient to break the bonds between Au and binding carbons and for Au to move between stable sites (at the edges or defects of graphene) more easily than Pt moving between carbons.[23,56] Because Au single atoms that move on the edges of graphene and nanographene have a high probability of meeting and aggregating, aggregated Au nanoparticles were also found on the edges. Figure 10(b) confirms this assumption.

Owing to its high catalytic properties, researchers have made efforts to make Au into finer particles.[6,7,57-63] For practical use, several methods have been developed, such as the coprecipitation method, the deposition–precipitation method, and the cathodic arc plasma deposition method, and they have succeeded in forming Au nanoparticles that are several nanometers.[9] The ultimate fine particle is a single atom, but the atomization of Au is difficult by these methods. The atomization of Au has been achieved by the sputtering method,[23] but the Au single atom is not stable because it moves considerably under electron beam irradiation. Thus, single atoms of Au have been developed to stabilize the single atomic state by using a covalent metal–support interaction method, such as FeOx.[1] In this study, we succeeded in atomizing Au by the sputtering method developed by our research group,[14,21] and we experimentally evaluated the mobility of Au single atoms on graphene by comparing it with that of Pt single atoms. Then, we found that Au single atoms tended to agglomerate upon electron beam irradiation to the extent that the nanoparticles are put into practical use. By utilizing this property, we believe that it is possible to create particles of any size from single atoms to nanoparticles.

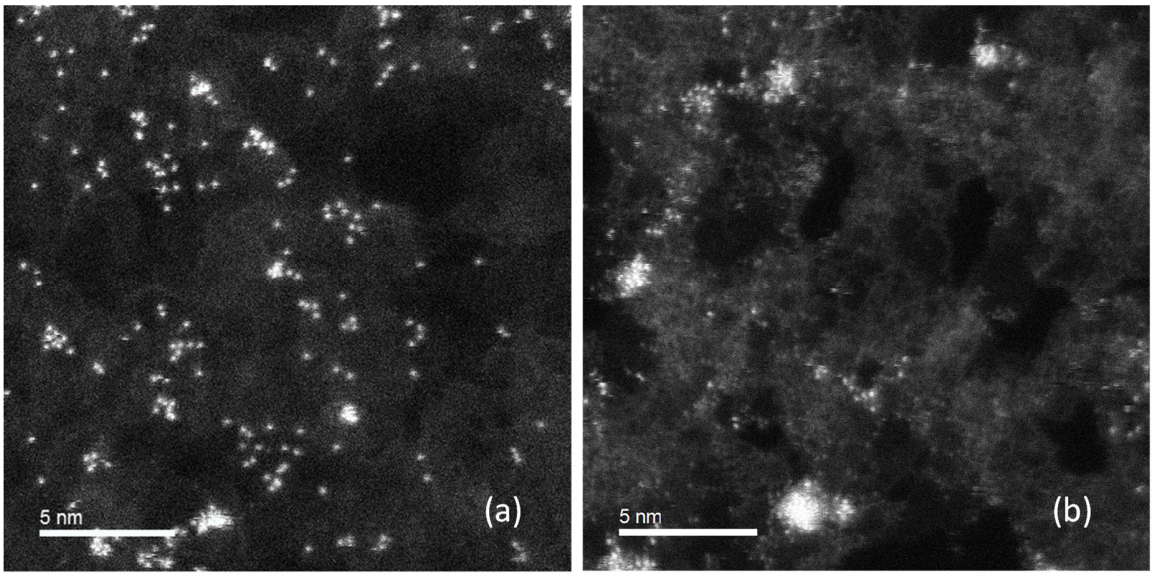

Figure 10. Low-magnification (×10M) STEM images of (a) Pt-dispersed graphene and (b) Au dispersed graphene. The acceleration voltage for STEM observation was 80 kV.

Conclusions

In this study, platinum (Pt) and gold (Au) single atoms dispersed on free-standing monolayer graphene were continuously observed via aberration-corrected scanning transmission microscopy (STEM), and the difference in the dynamic behavior of the single atoms on graphene under electron beam irradiation was observed. Analysis was performed after the drift corrections to track the movement of the metal atoms from their binding sites with angstrom-order accuracy.

STEM was performed continuously for 40 s in the same field of view, and we found that most of the Pt and Au single atoms were present at the nanographene edge. Approximately 80% of Pt single atoms traveled less than the nearest carbon atom distance of graphene (1.4 Å) during the observation interval (10 s). This remained unchanged during our observation (40 s), with an average of 8.3 (±5.4) × 10^{-12} m/s for all particles. Thus, Pt was confirmed to be stably dispersed on the graphene as single atoms. However, Au atoms could be dispersed on graphene by the same method as that used with Pt, and they were present at the nanographene edge, like Pt. However, the Au single atom mobility was larger than that of Pt. More than 50% of the particles traveled a distance exceeding the size of the six-membered ring of graphene (2.8 Å) during the minimum observation interval (4 s), and the variation in moving distance during the observation time was large (the average of all Au particles was 1.2 (±0.9) × 10^{-10} m/s. The mean square displacements (MSDs) of metal atoms also showed similar trends. The increasing rate of MSD of Pt (1.0 × 10^{-3} nm^2/s) was one-order smaller than that of Au (1.2 × 10^{-2} nm^2/s).

Upon analyzing the three-dimensional structure of nanographene, we found that these single metal atoms were mainly present on more than three-layer nanographene, and almost no atoms were found on the terrace of first layer graphene. One reason for this result is that the higher-

layer nanographene has many binding sites for metal atoms because it is structurally unstable and has many defects and edges compared with lower-layered nanographene.

In the future, it will be important to study the stabilization mechanism of each single atom of Pt and Au on graphene by combining experimental results and quantitative evaluation by computational methods. Furthermore, by using the in situ observation/analysis method developed in this study, it will be possible to observe the stability of single metal atoms under different environments and study the agglomeration of single atoms into nanoparticles.

ASSOCIATED CONTENT

Supporting Information

Identification of Pt and Au single atoms on free-standing graphene by HAADF-image analysis and EELS measurements (PDF)

Continuous observation images of Pt and Au dispersed graphene samples in normal image and with pseudo-colored nanographene layer structure image (AVI)

AUTHOR INFORMATION

Corresponding Author

E-mail: t-uchida@eng.hokudai.ac.jp (T. U.), orcid.org/0000-0003-2304-376X

Present Addresses

[+] Tome R&D Inc., Keihanna Lab. Bldg. 13F, Hikaridai 1-7, Seika-cho, Souraku-gun, Kyoto 619-0237, Japan

Author Contributions

K. Y., K. G. and T. U. conceived the idea and designed the study. A. S. and K. Y. performed the sample preparations and the STEM observations, and K. G. and T. U. analyzed the TEM/STEM data. A. S. and T. U. wrote the manuscript. All the authors contributed to and commented on the manuscript.

Notes

Any additional relevant notes should be placed here.

ACKNOWLEDGMENT

This work was partly supported by a JSPS Grant-in-Aid for Scientific Research (grants 26105009, 19K1543909, and 20K15165). A part of this work was conducted at Hokkaido University and was supported by the Nanotechnology Platform Program of the Ministry of Education, Culture, Sports, Science, and Technology (MEXT), Japan. The authors acknowledge Mr. Ohta for his assistance operating the STEM facility, and Ms. Sawamoto for her technical supports of sample preparations. We would also like to thank Enago (www.enago.jp) for the English language review.

ABBREVIATIONS

STEM, scanning transmission electron microscope: HAADF, high-angle annular dark-field; CVD, chemical vapor deposition; EELS, Electron Energy Loss Spectroscopy; ZNCC, zero-mean normalized cross-correlation; FMHW, full width at half maximum.

REFERENCES

(1) Qiao, B.; Liang, J. X.; Wang, A.; Xu, C. Q.; Li, J.; Zhang, T.; Liu, J. Ultrastable Single-Atom Gold Catalysts with Strong Covalent Metal-Support Interaction (CMSI), *Nano Res.* **2015**, 8 (9), 2913–2924. doi: 10.1007/212274-015-0796-9.

(2) Trasatti, S. Work Function, Electronegativity, and Electrochemical Behaviour of Metals: III. Electrolytic Hydrogen Evolution in Acid Solutions, *J. Electroanal. Chem. Interfacial Electrochem.* **1972**, 39 (1), 163–184. doi: 10.1016/S0022-0728(72)80485-6

(3) Mao, Y.; Chen, J.; Wang, H.; Hu, P. Catalyst Screening: Refinement of the Origin of the Volcano Curve and Its Implication in Heterogeneous Catalysis, *Chin. J. Catal.* **2015**, 36 (9), 1596–1605. doi: 10.1016/S1872-2067(15)60875-0

(4) Cheng, N.; Stambula, S.; Wang, D.; Banis, M. N.; Liu, J.; Riese, A.; Xiao, B.; Li, R.; Sham, T. K.; Liu, L. M. et al. Platinum Single-Atom and Cluster cCatalysis of the Hydrogen Evolution Reaction, *Nat. Commun.* **2016**, 7, 13638. doi: 10.1038/ncomms13638.

(5) Ye, T. N.; Xiao, Z.; Li, J.; Gong, Y.; Abe, H.; Niwa, Y.; Sasase, M.; Kitano, M.; Hosono, H. Stable Single Platinum Atoms Trapped in Sub-Nanometer Cavities in 12 $CaO \cdot 7Al_2O_3$ for Chemoselective Hydrogenation of Nitroarenes, *Nat. Commun.* **2020**, 11, 1020. doi: 10.1038/s41467-019-14216-9.

(6) Haruta, M.; Yamada, N.; Kobayashi, T.; Iijima, S. Gold Catalysts Prepared by Coprecipitation for Low-Temperature Oxidation of Hydrogen and of Carbon Monoxide, *J. Catal.* **1989**, 115 (2), 301–309. doi: 10.1016/0021-9517(89)90034-1

(7) Haruta, M. Role of Perimeter Interfaces in Catalysis by Gold Nanoparticles, *Faraday Discuss.* **2011**, 152, 11–32. doi: 10.1039/C1FD00107H

(8) Kumar, S.; Selvaraj, C.; Munichandraiah, N.; Scanlon, L. G. Gold Nanoparticles Anchored Reduced Graphene Oxide as Catalyst for Oxygen Electrode of Rechargeable Li-O_2 Cells, *RSC Adv.* **2013**, 3, 21706–21714. doi: 10.1039/C3RA42617C

(9) Okumura, M.; Fujitani, T.; Huang, J.; Ishida, T. A Career in Catalysis: Masatake Haruta, *ACS Cat.* **2015**, 5, 4699–4707. doi: 10.1021/acscatal.5b01122.

(10) Remediakis, I. N.; Lopez, N.; Norskov, J. K. CO Oxidation on Rutile-Supported Au Nanoparticles, *Angew. Chem. Int. Ed.* **2005**, 44, 1824–1826. doi: 10.1002/anie.200461699.

(11) Yang, X. F.; Wang, A.; Qiao, B.; Li, J.; Liu, J. Y.; Zhang, T. Single-Atom Catalysts: A New Frontier in Heterogeneous Catalysis. *Acc. Chem. Res.* **2013**, 46, 1740–1748. doi: 10.1021/ar300361 m

(12) Castro Neto, A. H.; Guinea, F.; Peres, N. M. R.; Novoselov, K. S.; Geim, A. K. The Electronic Properties of Graphene, *Rev. Mod. Phys.* **2009**, 81 (1), 109–162. doi: 10.1103/RevModPhys.81.109.

(13) Papageorgiou, D. G.; Kinloch, I. A.; Young, R. J. Mechanical Properties of Graphene and Graphene-Based Nanocomposites, *Prog. Mater. Sci.* **2017**, 90, 75–127. doi: 10.1016/j.pmatsci.2017.07.004.

(14) Yamazaki, K.; Maehara, Y.; Kitajima, R.; Fukami, Y.; Gohara, K. High-Density Dispersion of Single Platinum Atoms on Graphene by Plasma Sputtering in N_2 Atmosphere, *Appl. Phys. Express* **2018**, 11 (9), 095101. doi: 10.7567/APEX.11.095101.

(15) Wang, H.; Wang, Q.; Cheng, Y.; Li, K.; Yao, Y.; Zhang, Q.; Dong, C.; Wang, P.; Schwingenschögl, U.; Yang, W.; Zhang, X. X. Doping Monolayer Graphene with Single Atom Substitutions, *Nano Lett.* **2012**, 12 (1), 141–144. doi: 10.1021/nl2031629.

(16) Bolotin, K. I.; Sikes, K. J.; Jiang, Z.; Klima, M.; Fudenberg, G.; Hone, J.; Kim, P.; Stormer, H. L. Ultrahigh Electron Mobility in Suspended Graphene, *Solid State Commun.* **2008**, 146 (9–10), 351–355. doi: 10.1016/j.ssc.2008.02.024.

(17) Lee, C.; Wei, X.; Kysar, J. W.; Hone, J. Measurement of the Elastic Properties and Intrinsic Strength of Monolayer Graphene, *Science* **2008**, 321, 385–388. doi: 10.1126/science.1157996

(18) Li, X.; Cai, W.; An, J.; Kim, S.; Nah, J.; Yang, D.; Piner, R.; Velamakanni, A.; Jung, I.; Tutuc, E. et al. Large-Area Synthesis of High-Quality and Uniform Graphene Films on Copper Foils, *Science* **2009**, 324 (5932), 1312–1314. doi: 10.1126/science.1171245.

(19) Hao, Y.; Bharathi, M. S.; Wang, L.; Liu, Y.; Chen, H.; Nie, S.; Wang, X.; Chou, H.; Tan, C.; Fallahazad, B. et al. The Role of Surface Oxygen in the Growth of Large Single-Crystal Graphene on Copper, *Science* **2013**, 342 (6159), 720–723. doi: 10.1126/science.1243879.

(20) Maehara, Y.; Yamazaki, K.; Gohara, K. Nanographene Growing on Free-Standing Monolayer Graphene, *Carbon* **2018**, 143, 669–677. doi: 10.1016/j.carbon.2018.11.025

(21) Yamazaki, K.; Maehara, Y.; Lee, C. C.; Yoshinobu, J.; Ozaki, T.; Gohara, K. Atomic Sructure and Local Electronic States of Single Pt Atoms Dispersed on Graphene, *J. Phys. Chem. C* **2018**, 122, 48, 27292–27300,. doi: 10.1021/acs.jpcc.8b04529

(22) Lu, J.; Aydin, C.; Browning, N. D.; Gates, B. C. Imaging Isolated Gold Atom Catalytic Sites in Zeolite NaY, *Angew. Chem. Int. Ed. Engl.* **2012**, 51, 5842–5846. doi: 10.1002/anie.201107391.

(23) Wang, H.; Li, K.; Cheng, Y.; Wang, Q.; Yao, Y.; Schwingenschlögl, U.; Zhang, X.; Yang, W. Interaction Between Single Gold Atom and the Graphene Edge: A Study via Aberration-Corrected Transmission Electronmicroscopy, *Nanoschale* **2012**, 4, 2920–2925. doi: 10.1039/c2nr00059h.

(24) Hardcastle, T. P.; Seabourne, C. R.; Zan, R.; Brydson, R. M. D.; Bangert, U.; Ramasse, Q. M.; Novoselov, K. S.; Scott, A. J. Mobile Metal Adatoms on Single Layer, Bilayer, and Trilayer Graphene: An ab initio DFT Study with van der Waals Corrections Correlated with Electron Microscopy Data, *Phys. Rev. B* **2013**, 87, 195430. doi: 10.1103/PhysRevB.87.195430.

(25) Trentino, A.; Mizohata, K.; Zagler, G.; Längle, M.; Mustonen, K.; Susi, T.; Kotakoski, J.; Åhlgren, E. H. Two-Step Implantation of Gold into Graphene. *2D Mater*., **2022**, 9, 025011. doi: 10.1088/2053-1583/ac4e9c

(26) Ramasse, Q. M.; Zan, R.; Bangert, U.; Boukhvalov, D. W.; Son, Y. W.; Novoselov, K. S. Direct Experimental Evidence of Metal-Mediated Etching of Suspended Graphene, *ACS Nano* **2012**, 6 (5), 4063–4071. doi: 10.1021/nn300452y.

(27) Lin, Y.-C.; Teng, P.-Y.; Chiu, P.-W.; Suenaga, K. Exploring the Single Atom Spin State by Electron Spectroscopy. *Phys. Rev. Lett.*, **2015**, 115, 206803. doi: 10.1103/PhysRevLett.115.206803.

(28) Dyck, O.; Yoon, M.; Zhang, L.; Lupini, A.R.; Swett, J.L.; Jesse, S. Doping of Cr in Graphene Using Electron Beam Manipulation for Functional Defect Engineering. *ACS Appl. Nano Mater*., **2020**, 3, 10855–10863. doi: 10.1021/acsanm.0c02118.

(29) Dyck, O.; Zhang, L.; Yoon, M.; Swett, J.L.; Hensley, D.; Zhang, C.; Rack, P.D.; Fowlkes, J.D.; Lupini, A.R.; Jesse, S. Doping Transition-Metal Atoms in Graphene for Atomic-Scale Tailoring of Electronic, Magnetic, and Quantum Topological Properties. *Carbon*, **2021**, 173, 205–214. doi: 10.1016/j.carbon.2020.11.015.

(30) Robertson, A. W.; Moun;tanari, B.; He, K.; Kim, J.; Allen, C. S.; Wu, Y. A.; Olivier, J.; Neethling, J.; Harrison, N.; Kirkland, A. I. et al. Dynamics of Single Fe Atoms in Graphene Vacancies, *Nano Lett.* **2013**, 13, 1468–1475. doi: 10.1021/nl304495v.

(31) Furnival, T.; Leary, R. K.; Tyo, E. C.; Vajda, S.; Ramasse, Q. M.; Thomas, J. M.; Bristowe, P. D.; Midgley, P. A. Anomalous diffusion of single metal atoms on a graphene oxide support, *Chem. Phys. Lett.* **2017**, 683, 370–374. doi: 10/1017/j.cplett.2017.04.071.

(32) Dyck, O.; Kim, S.; Kalinin, S.V.; Jesse, S. Placing single atoms in graphene with a scanning transmission electron microscope, *Appl. Phys. Lett.* **2017**, 111, 113104. doi: 10.1063/1.4998599.

(33) Dyck, O.; Zhang, C.; Rack, P.D.; Fowlkes, J.D.; Sumpter, B.; Lupini, A.R.; Kalinin, S.V.; Jesse, S. Electron-beam introduction of heteroatomic Pt–Si structures in graphene. *Carbon*, **2020**, 161, 750–757. doi: 10.1016/j.carbon.2020.01.042.

(34) Elibol, K.; Mangler, C.; O'Regan, D.D.; Mustonen, K.; Eder, D.; Meyer, J.C.; Kotakoski, J.; Hobbs, R.G.; Susi, T.; Bayer, B.C. Single Indium Atoms and Few-Atom Indium Clusters

Anchored onto Graphene via Silicon Heteroatoms. *ACS Nano*, **2021**, 15, 14373–14383. doi: 10.1021/acsnano.1c03535.

(35) Tripathi, M.; Markevich, A.; Böttger, R.; Facsko, S.; Besley, E.; Kotakoski, J.; Susi, T. Implanting Germanium into Graphene. *ACS Nano*, **2018**, 12, 4641–4647. doi: 10.1021/acsnano.8b01191.

(36) Susi, T.; Hardcastle, T.P.; Hofsäss, H.; Mittelberger, A.; Pennycook, T.J.; Mangler, C.; Drummond-Brydson, R.; Scott, A.J.; Meyer, J.C.; Kotakoski, J. Single-Atom Spectroscopy of Phosphorus Dopants Implanted into Graphene. *2D Materials*, **2017**, 4, 021013.

(37) Sugimoto, R.; Segawa, Y.; Suzuta, A.; Kunisada, Y.; Uchida, T.; Yamazaki, K.; Gohara, K. Single Pt Atoms on N-Doped Graphene: Atomic Structure and Local Electronic States, *J. Phys. Chem. C* **2021**, 125 (5), 2900–2906 doi: 10.1021/acs.jpcc.0c08811

(38) Gan, Y.; Sun, L.; Banhart, F. One- and Two-Dimensional Diffusion of Metal Atoms in Graphene, *Small* **2008**, 4 (5), 587-591. doi: 10.1002/small.200700929.

(39) Mukherjee, S.; Ramalingam, B.; Gangopadhyay, K.; Gangopadhyay, S. Stability of Sub--2 nm Pt Nanoparticles on Different Support Surfaces, *J. Electrochem. Soc.* **2014**, 161 (4), F493–F499. doi: 10.1149/2.071404jes.

(40) Qiao, B.; Wang, A.; Yang, X.; Allard, L. F.; Jiang, Z.; Cui, Y.; Liu, J.; Li, J.; Zhang, T. Single-Atom Catalysis of CO Oxidation Using Pt_1/FeO_x, *Nat. Chem.* **2011**, 3, 634–641. doi: 10.1038/nchem.1095

(41) Sun, S.; Zhang, G.; Gauquelin, N.; Chen, N.; Zhou, J.; Yang, S.; Chen, W.; Meng, X.; Geng, D.; Banis, M. N. et al. Single-Atom Catalysis Using Pt/Graphene Achieved Through Atomic Layer Deposition, *Sci. Rept.* **2013**, 3, 1775. doi: 10.1038/srep01775.

(42) Zan, R.; Bangert, U.; Ramasse, Q.; Novoselov, K. S. Metal-Graphene Interaction Studied via Atomic Resolution Scanning Transmission Electron Microscopy, *Nano Lett.* **2011**, 11, 1087–1092. doi: 101021/nl103980h.

(43) Pandey, P. A.; Bell, G. R.; Rourke, J. P.; Sanchez, A. M.; Elkin, M. D.; Hickey, B. J.; Wilson, N. R. Physical Vapor Deposition of Metal Nanoparticles on Chemically Modified Graphene: Observations on Metal-Graphene Interactions, *Small* **2011**, 7 (22), 3202–3210. doi: 10.1002/small.201101430.

(44) Sun, X.; Dawson, S. R.; Permentier, T. E.; Malta, G.; Davies, T. E.; He, Q.; Lu, L.; Morgan, D. J.; Carthey, N.; Johnston, P. et al. Facile Synthesis of Precious-Metal Single-Site Catalysts Using Organic Solvents, *Nat. Chem.* **2020**, 12, 560. doi: 10.1038/s41557-020-0446-z

(45) Zhuo, H. Y.; Zhang, X.; Liang, J. X.; Yu, Q.; Xiao, H.; Li, J. Theoretical Understandings of Graphene-Based Metal Single-Atom Catalysts: Stability and Catalytic Performance, *Chem. Rev*. **2020**, 120, 12315–12341. doi: 10.1021/acs.chemrev.0c00818

(46) Yamazaki, K.; Maehara, Y.; Gohara, K. Characterization of TEM Moiré Patterns Originating from Two Monolayer Graphenes Grown on the Front and Back Sides of a Copper Substrate by CVD Method, *J. Phys. Soc. Jpn.* **2018**, 87, 061011. doi: 10.7566/JPSI.87.061011.

(47) Meyer, J. C.; Kisielowski, C.; Erni, R.; Rossell, M. D.; Crommie, M. F.; Zettl, A. Direct Imaging of Lattice Atoms and Topological Defects in Graphene Membranes, *Nano Lett.* **2008**, 8, 3582–3586. doi: 10.1021/nl801386 m.

(48) Meyer, J. C.; Eder, F.; Krasch, S.; Skakalova, V.; Kotakoski, J.; Park, H. J.; Roth, S.; Chuvilin, A.; Evhusen, S.; Benner, G. et al. Accurate Measurement of Electron Beam Induced Displacement Cross Sections for Single-Layer Graphene. Phys. Rev. Lett., 2012, 108, 196102. doi: 10.1103/PhysRevLett.108.196102.

(49) Segawa, Y.; Yamazaki, K.; Yamasaki, J.; Gohara, K. Quasi-Static 3D Structure of Graphene Ripple Measured Using Aberration-Corrected TEM, *Nanoscale* **2021**, 13, 5847–5856. doi: 10.1039/d1nr00237f.

(50) Schindelin, J.; Arganda-Carreras, I.; Frise, E.; Kaynig, V.; Longair, M.; Pietzsch, T.; Preibisch, S.; Rueden, C.; Saalfeld, S.; Schmid, B. et al. Fiji: An Open-Source Platform for Biological-Image Analysis, *Nat. Methods* **2012**, 9 (7), 676–682. doi: 10.1038/nmeth.2019.

(51) Pennycook, S.J. Z-Contrast Stem for Materials Science. *Ultramicroscopy*, **1989**, 30, 58–69. doi: 10.1016/0304-3991(89)90173-3.

(52) Krivanek, O.L.; Chisholm, M.F.; Nicolosi, V.; Pennycook, T.J.; Corbin, G.J.; Dellby, N.; Murfitt, M.F.; Own, C.S.; Szilagyi, Z.S.; Oxley, M.P., et al. Atom-by-Atom Structural and Chemical Analysis by Annular Dark-Field Electron Microscopy. *Nature*, **2010**, 464, 571–574.

(53) Steel, R.G.D. A Rank Sum Test for Comparing All Pairs of Treatments, *Technometrics* **1960**, 2 (2), 197-207. doi: 10.1080/00401706.1960.10489894.

(54) Hasegawa, S.; Kunisada, Y.; Sakaguchi, N. Diffusion of A Single Platinum Atom on Light-Element-Doped Graphene, *J. Phys. Chem. C* **2017**, 121 (33), 17787–17795. doi: 10.1021/acs.jpcc.7b01241.

(55) Maiti, A.; Ricca, A. Metal-Nanotube Interactions–Binding Energies and Wetting Properties, *Chem. Phys. Lett*. **2004**, 395, 7–11. doi: 10.1016/j.cplett.2004.07.024.

(56) Zhang, Z.; Chen, Y.; Zhou, L.; Chen, C.; Han, Z.; Zhang, B.; Wu, Q.; Yang, L.; Du, L.; Bu, Y. et al. The Simplest Construction of Single-Site Catalysts by the Synergism of Micropore Trapping and Nitrogen Anchoring, *Nat. Comm.* **2019**, 10, 1657. doi: 10.1038/s41467-019-09596-x

(57) Chen, M. S.; Goodman, D. W. The Structure of Catalytically Active Gold on Titania. *Science* **2004**, 306, 252–255. doi: 10.1126/science.1102420

(58) Herzing, A. A.; Kiely, C. J.; Carley, A. F.; Landon, P.; Hutchings, G. J. Identification of Active Gold Nanoclusters on Iron Oxide Supports for CO Oxidation, *Science* **2008**, 321, 1331–1335. doi: 10.1126/science.1159639

(59) Turner, M.; Golovko, V. B.; Vaughan, O. P. H.; Abdulkin, P.; Berenguer-Murcia, A.; Tikhov, M. S.; Johnson, B. F. G.; Lambert, R. M. Selective Oxidation with Dioxygen by Gold Nanoparticle Catalysts Derived from 55-Atom Clusters, *Nature* **2008**, 454, 981–983. doi: 10.1038/nature07194

(60) Haruta, M. When Gold is Not Noble: Catalysis by Nanoparticles, *Chem. Record* **2003**, 3, 75–87. doi: 10.1002/tcr.10053

(61) Hughes, M. D.; Xu, Y. J.; Jenkins, P.; McMorn, P.; Landon, P.; Enache, D. I.; Carley, A. F.; Attard, G. A.; Hutchings, G. J.; King, F. et al. Tunable Gold Catalysts for Selective Hydrocarbon Oxidation under Mild Conditions, *Nature* **2005**, 437, 1132–1135. doi: 10.1038/nature04190

(62) Corma, A.; Serna, P. Chemoselective Hydrogenation of Nitro Compounds with Supported Gold Catalysts, *Science* **2006**, 313, 332–334. doi: 10.1126/science.1128383

(63) Ball, L. T.; Lloyd-Jones, G. C.; Russell, C. A. Gold-Catalyzed Direct Arylation. *Science* **2012**, 337, 1644–1648. doi: 10.1126/science.1225709